Applied Radiation and Isotopes 186 (2022) 110252

Contents lists available at ScienceDirect

Applied Radiation and Isotopes

journal homepage: www.elsevier.com/locate/apradiso

# Optimization of $^{68}$Ga production at an 18 MeV medical cyclotron with solid targets by means of cross-section measurement of $^{66}$Ga, $^{67}$Ga and $^{68}$Ga

S. Braccini [a,*], T.S. Carzaniga [a,1], G. Dellepiane [a], P.V. Grundler [b], P. Scampoli [a,c], N.P. van der Meulen [b,d], D. Wüthrich [a,2]

[a] Albert Einstein Center for Fundamental Physics (AEC), Laboratory for High Energy Physics (LHEP), University of Bern, Sidlerstrasse 5, CH-3012 Bern, Switzerland
[b] Center for Radiopharmaceutical Sciences ETH-PSI-USZ, Paul Scherrer Institute, Forschungstrasse 111, 5232 Villigen-PSI, Switzerland
[c] Department of Physics "Ettore Pancini", University of Napoli Federico II, Complesso Universitario di Monte S. Angelo, 80126 Napoli, Italy
[d] Laboratory of Radiochemistry, Paul Scherrer Institute, Forschungstrasse 111, 5232 Villigen-PSI, Switzerland

ARTICLE INFO

*Keywords:*
PET
Ga-68
Cross-section
Solid target
Medical cyclotrons
Theranostics

ABSTRACT

The future development of personalized nuclear medicine relies on the availability of novel medical radionuclides. In particular, radiometals are attracting considerable interest since they can be used to label both proteins and peptides. Among them, the $\beta^+$-emitter $^{68}$Ga is widely used in nuclear medicine for positron emission tomography (PET). It is used in theranostics as the diagnostic partner of the therapeutic $\beta^-$-emitters $^{177}$Lu and $^{90}$Y for the treatment of a wide range of diseases, including prostate cancer. Currently, $^{68}$Ga is usually obtained via $^{68}$Ge/$^{68}$Ga generators. However, their availability, high price and limited produced radioactivity per elution are a major barrier for a wider use of the $^{68}$Ga-based diagnostic radiotracers. A promising solution is the production of $^{68}$Ga by means of proton irradiation of enriched $^{68}$Zn liquid or solid targets. Along this line, a research program is ongoing at the Bern medical cyclotron, equipped with a solid target station. In this paper, we report on the measurements of $^{68}$Ga, $^{67}$Ga and $^{66}$Ga production cross-sections using natural Zn and enriched $^{68}$Zn material, which served as the basis to perform optimized $^{68}$Ga production tests with enriched $^{68}$Zn solid targets.

## 1. Introduction

Radiometals play a fundamental role in the future development of personalized nuclear medicine. The interest in this class of radionuclides concerns both the fields of diagnostics and therapy and is based on their possibility to label relevant bio-molecules such as proteins and peptides.

$^{68}$Ga ($t_{1/2}$ = 67.7 min, $\beta^+$: 88.9% IAEA, 2021) is used to label PSMA ligands (e.g. PSMA-11) to diagnose prostate cancer and somatostatin analogues (e.g. DOTATOC, DOTATATE) to diagnose NeuroEndocrine Tumors (NET). A therapeutic partner of $^{68}$Ga is the $\beta^-$-emitter $^{177}$Lu, which labels the same peptide ligand (e.g. $^{177}$Lu-DOTATATE). This pair is widely used for NET treatment.

Currently, $^{68}$Ga is obtained via $^{68}$Ge/$^{68}$Ga generators. The parent radionuclide $^{68}$Ge has a half-life of 271 days, which makes it possible to use such a generator for about one year. Although this technology is widely used, it presents some non-optimal features such as the limited produced activity (typically up to 2.4 GBq nominal activity per elution for a new generator), the minimum interval between elutions (typically 3–4 h), the maximum number of elutions (up to 450), the elution efficiency (60%–70%) and the risk of contamination of the eluted solution by the long-lived $^{68}$Ge impurity due to a possible breakthrough from the generator column. Furthermore, the high price of the generators and their limited availability represent a major impediment for a wider adoption of $^{68}$Ga-based diagnostic radiotracers. In particular, the use of $^{68}$Ga might become not economical in small nuclear medicine departments treating a limited number of patients or, in larger hospitals, when a single generator is not sufficient and a second one is needed, almost doubling the costs (IAEA, 2019).

To overcome this limitation, cyclotron production could be a valid alternative (IAEA, 2019). $^{68}$Ga can be obtained by proton irradiation from enriched $^{68}$Zn material, via the $^{68}$Zn(p,n)$^{68}$Ga nuclear reaction, using either liquid (Alves et al., 2017; Riga et al., 2018) or solid targets (Nelson et al., 2020; Alnahwi et al., 2020).

* Corresponding author.
*E-mail address:* saverio.braccini@lhep.unibe.ch (S. Braccini).
[1] Now at SWAN Isotopen AG, Bern, Switzerland.
[2] Now at Institute of Radiation Physics, Lausanne University Hospital, Switzerland.

https://doi.org/10.1016/j.apradiso.2022.110252
Received 28 February 2022; Received in revised form 31 March 2022; Accepted 19 April 2022
Available online 26 April 2022

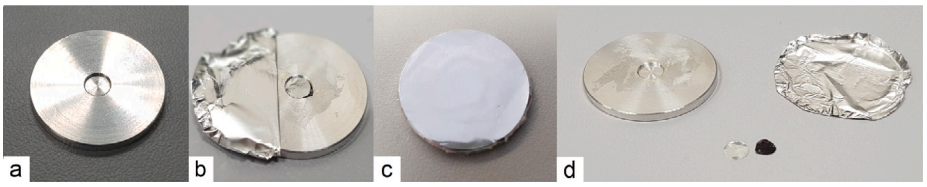


**Fig. 1.** Natural Zn target preparation procedure, using an aluminum disc as support. (a) aluminum disc with the pocket housing the target; Disc with aluminum cover before (b) and after (c) gluing; (d) the target disassembled after irradiation: the disc with the foil, the Zn target and a radiochromic film sometimes used instead of the Zn target for beam diagnostics.

The main advantage of liquid target production lies in the possibility of using capillary systems similar to the consolidated ones used for $^{18}$F production for transferring the radioactivity to the radiopharmacy. This prevents the equipping of the cyclotron with a solid target station and a specific transfer system. This method also saves time in target preparation and post-irradiation dissolution. However, production yields are limited and often not significantly higher with respect to those obtained with generators (Nelson et al., 2020). On the other hand, the production by means of a solid target station allows the production of large activities of $^{68}$Ga, with reported yields of 5–6 GBq/μAh (Sadeghi et al., 2009), but presents several challenges such as the target preparation, the post-irradiation target handling, including the dissolution process, and the possible contamination from the support of the target material.

In the framework of a research program focused on novel radionuclides for theranostics at the Bern medical cyclotron laboratory (Braccini et al., 2019), $^{68}$Ga production was investigated via proton bombardment of metallic enriched $^{68}$Zn solid targets.

The most important impurities to be kept under control are $^{67}$Ga, obtained from $^{68}$Zn and $^{67}$Zn via the $^{68}$Zn(p,2n)$^{67}$Ga and $^{67}$Zn(p,n)$^{67}$Ga reactions, respectively, and $^{66}$Ga, obtained from $^{67}$Zn and $^{66}$Zn via $^{67}$Zn(p,2n)$^{66}$Ga and $^{66}$Zn(p,n)$^{66}$Ga, respectively. To maximize $^{68}$Ga activities while minimizing $^{67}$Ga and $^{66}$Ga impurities, the precise knowledge of the reaction cross-sections as function of the beam energy is of paramount importance. Data reported in literature and accessible via the EXFOR database (https://www-nds.iaea.org/exfor/) do not fully cover the energy range of medical cyclotrons and are sometimes inconsistent. It has to be remarked that the European Pharmacopoeia requires a $^{68}$Ga fraction to be above 98% at injection time (Anon, 2021).

In this paper we report on the measurement of $^{68}$Ga, $^{67}$Ga and $^{66}$Ga production cross-sections, performed with the Beam Transfer Line (BTL) at the Bern medical cyclotron. These results were used to optimize the main parameters for the production of $^{68}$Ga by maximizing the radionuclidic purity and the production yield. On this basis, production irradiation tests from enriched $^{68}$Zn solid targets were performed using the solid target station in operation at the Bern medical cyclotron.

## 2. Materials and methods

The laboratory at the Bern University Hospital (Inselspital) (Braccini, 2013) features an IBA Cyclone 18/18 high current cyclotron (18 MeV proton beams, max. 150 μA extracted current, 8 exit ports), equipped with an IBA Nirta Solid Target Station (STS) and a 6-m-long external Beam Transfer Line (BTL), which brings the beam to a second bunker with an independent access.

This solution is unusual for a hospital-based facility and was conceived to pursue both multidisciplinary research activities (Braccini and Scampoli, 2016) and $^{18}$F-labeled PET tracer routine production, performed by the spin-off company SWAN Isotopen AG. In particular, the BTL was used for the cross-section measurements presented in this paper. The beam extracted to the BTL has a distribution with a mean energy of (18.3 ± 0.3) MeV and a Root Mean Square (RMS) of (0.4 ± 0.2) MeV (Häffner et al., 2019; Nesteruk et al., 2018).

**Table 1**
Isotopic fractions in natural Zn and enriched $^{68}$Zn target materials used in this study. (A) metallic zinc foil by TRACE Sciences International (www.tracesciences.com), (B) metallic zinc powder and (C) metallic zinc foil by ISOFLEX (www.isoflex.com). The values in parentheses are the uncertainties referred to the last digits of the value.

| | $^{64}$Zn | $^{66}$Zn | $^{67}$Zn | $^{68}$Zn | $^{70}$Zn |
|---|---|---|---|---|---|
| Natural [%] | 49.17 | 27.73 | 4.04 | 18.45 | 0.61 |
| 68-enr. [%] (A) | 0.99 | 0.81 | 0.38 | 97.80(20) | 0.02 |
| 68-enr. [%] (B) | 0.01 | 0.10 | 0.61 | 99.26(50) | 0.02 |
| 68-enr. [%] (C) | 0.53 | 0.44 | 0.30 | 98.70(20) | 0.03 |

### 2.1. Cross-section measurements

The experimental method used in this work was developed for previous studies on cross-section measurements and it is described in detail in Refs. Carzaniga et al. (2017), Carzaniga and Braccini (2019). It is based on the irradiation of the full mass of a thin target by a proton beam with a constant surface density. This method has the advantage that the target does not have to be necessarily uniform in thickness, provided that the energy of the protons can be considered constant within the mass of the target. The beam is flattened by the optical elements of the BTL and monitored online with the UniBEaM detector (Auger et al., 2016; Potkins et al., 2017), which is based on silica-doped fibers passing through the beam, allowing one to measure the beam profile in two dimensions.

A specific target station was designed and built for cross-section measurements. It provides a beam of controlled diameter by means of a collimator and is connected to an ammeter for measuring the current reaching the target. To obtain different impinging proton energies, the beam was degraded by means of aluminum attenuator discs placed in front of the target and its energy determined using the SRIM Monte Carlo code (Ziegler and Manoyan, 2013).

After each irradiation, the activity produced was measured by $\gamma$-spectroscopy. For this purpose, an N-type neutron resistant coaxial high-purity germanium (HPGe) detector was used (Canberra GR2009). The detector efficiency was assessed using a multi-peak $\gamma$-source, whose activity is known with an uncertainty of about 1%.

Cross-section measurements were performed using both natural and enriched $^{68}$Zn materials in the form of foils. For the production tests, foils as well as powder were used. Their isotopic compositions are reported in Table 1.

Natural zinc is available as a thin foil of 4 mm in diameter and 10 μm in thickness. It was placed in a 4.2-mm diameter and 0.8-mm deep pocket of an aluminum disc (22.8 mm in diameter, 2 mm thick), as shown in Fig. 1-a. The mass of each foil was assessed with an analytical scale (METTLER TOLEDO AX26 DeltaRange) with a sensitivity of 2 μg and a reproducibility of 4 μg. The pocket was sealed with a 13-μm thick aluminum foil glued or mechanically fixed to the disc (Figs. 1-b and c). This guarantees that the material is kept within the pocket throughout the irradiation and measurement procedure. In order to ensure that the whole target was hit by a flat beam, a radiochromic film with the same diameter as the targets was sometimes placed inside the pocket (Fig. 1-d).

The 97.80% enriched $^{68}$Zn zinc was provided by TRACE Science International as a 200 μm thick foil. The thickness was reduced to a

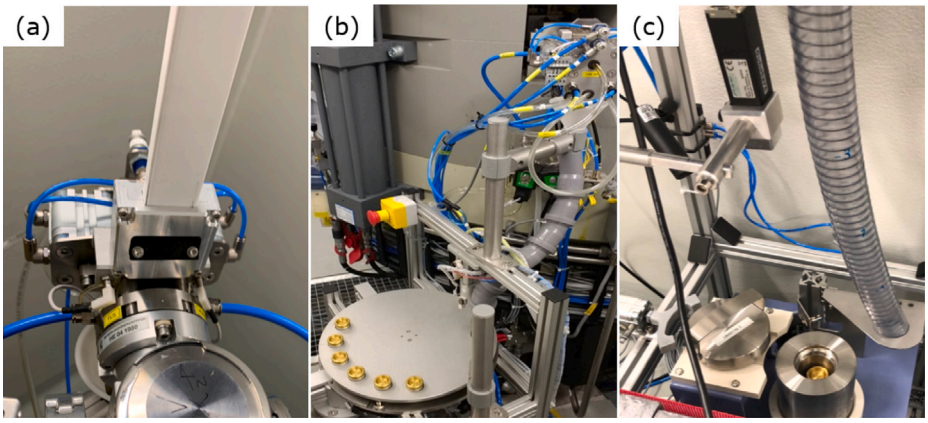


**Fig. 2.** (a) The Hyperloop connected to the STS. (b) The IBA Nirta solid target station and the Solid Target Transfer System (STTS). (c) The receiving station located in the BTL bunker.

**Table 2**
Investigated Ga radionuclides and their decay properties used for the measurement of their cross sections. The values in parentheses are the uncertainties referred to the last digits of the value. BR is the branching ratio.

| Radionuclide | $t_{1/2}$ | Decay mode [%] | $\gamma$ energy [keV] | BR [%] |
|---|---|---|---|---|
| $^{68}$Ga | 67.71(8) min | ec+$\beta^+$: 100 | 1077.34(5) | 3.22(3) |
| $^{67}$Ga | 3.2617(5) d | ec: 100 | 93.310(5) | 38.81(3) |
| $^{66}$Ga | 9.49(3) h | ec+$\beta^+$: 100 | 1039.220(3) | 37.0(20) |

few tens of μm by means of a press, so that the beam energy could be considered constant over the full irradiated mass. Finally, discs of about 4 mm in diameter were cut and targets prepared, as in the case of natural zinc.

In both cases, irradiations were performed at several entry energies with currents of about 10 nA for about 5 minutes. Natural zinc targets were measured with the HPGe detector immediately after the end of irradiation, while enriched zinc samples were measured repeatedly to exploit the difference in half-lives of the radionuclides of interest. In all measurements, the dead time was below 2%. The $\gamma$-lines used to identify the radionuclides of interest are listed in Table 2. To avoid unwanted contributions coming from zinc impurities in the aluminum support disc, the foil was removed from the support for the measurement of the activity.

As explained in the introduction, the production of $^{66}$Ga and $^{67}$Ga is the result of two nuclear reaction processes, namely, the (p,n) and the (p,2n). To disentangle the two contributions to the production cross-section, a method based on the inversion of a linear system of equations was applied. For a given beam energy, the production cross-section is measured for two different known enrichment levels. For the case of $^{67}$Ga the following linear system holds:

$$\begin{cases} \sigma\left({}^{nat}Zn(p,x)^{67}Ga\right) \\ \quad = \epsilon_{67}^{nat}\cdot\sigma\left({}^{67}Zn(p,n)^{67}Ga\right) + \epsilon_{68}^{nat}\cdot\sigma\left({}^{68}Zn(p,2n)^{67}Ga\right) \\ \sigma\left({}^{enr}Zn(p,x)^{67}Ga\right) \\ \quad = \epsilon_{67}^{enr}\cdot\sigma\left({}^{67}Zn(p,n)^{67}Ga\right) + \epsilon_{68}^{enr}\cdot\sigma\left({}^{68}Zn(p,2n)^{67}Ga\right) \end{cases} \quad (1)$$

where the experimentally-measured production cross sections appear on the left side of the equations and the reaction cross sections to be determined on the right. $\epsilon_i^{nat}$ and $\epsilon_i^{enr}$ are the isotopic abundances of the $i$th isotope for the natural and the enriched $^{68}$Zn material, respectively. An analogous system of equations holds for the case of $^{66}$Ga.

### 2.2. $^{68}$Ga production tests

The Solid Target Station (STS) installed directly in one out-port of the cyclotron was used for the production tests. To minimize the dose to the personnel, a mechanical transfer system (named Hyperloop, Fig. 2-a) was developed and installed to load the target station without entering the cyclotron bunker. The STS was customized with a pneumatic target transfer system (STTS) by TEMA Sinergie (Fig. 2-b) to send the shuttle containing the irradiated target either to one hot cell in the nearby GMP radiopharmacy, or to a receiving station located in the BTL bunker (Fig. 2-c). The latter option is used for all non-GMP activities and when the irradiated target is transported to external research laboratories for chemical processing.

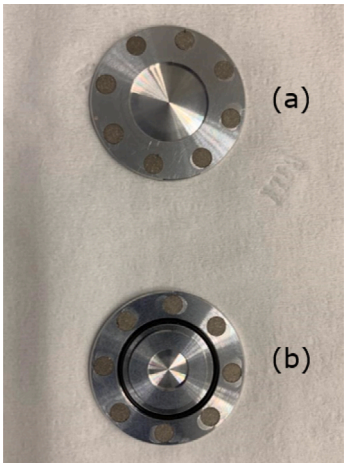


**Fig. 3.** The lid (a) and the cup (b) of the coin target (24-mm diameter, 2-mm thickness). The cup contains the pocket for the target and the O-ring.

The STS was designed to bombard target materials electroplated on a platinum or gold disc, 24 mm in diameter and 2 mm thick. During irradiation, the face of the disc hit by the beam is cooled by helium, while the back part is cooled by water.

Many interesting radiometals can be obtained from materials that cannot be electro-deposited but are available as powder. For this purpose, a specific magnetic "coin" target disc was conceived and built to irradiate compressed powder pellets or solid foils. With this method, several radionuclides have been produced (Dellepiane et al., 2021), in particular $^{44}$Sc (van der Meulen et al., 2020) and $^{155}$Tb (Favaretto et al., 2021; Dellepiane et al., 2022). The "coin", shown in Fig. 3, has the same external dimensions as an ordinary disc but is composed by two halves, the lid and the cup, kept together by small permanent magnets. The energy of the protons reaching the target material was set by adjusting the thickness of the lid, in order to optimize the activity produced and the radionuclidic purity. The cup hosts the 6-mm-diameter target and an O-ring to prevent the possible leakage of

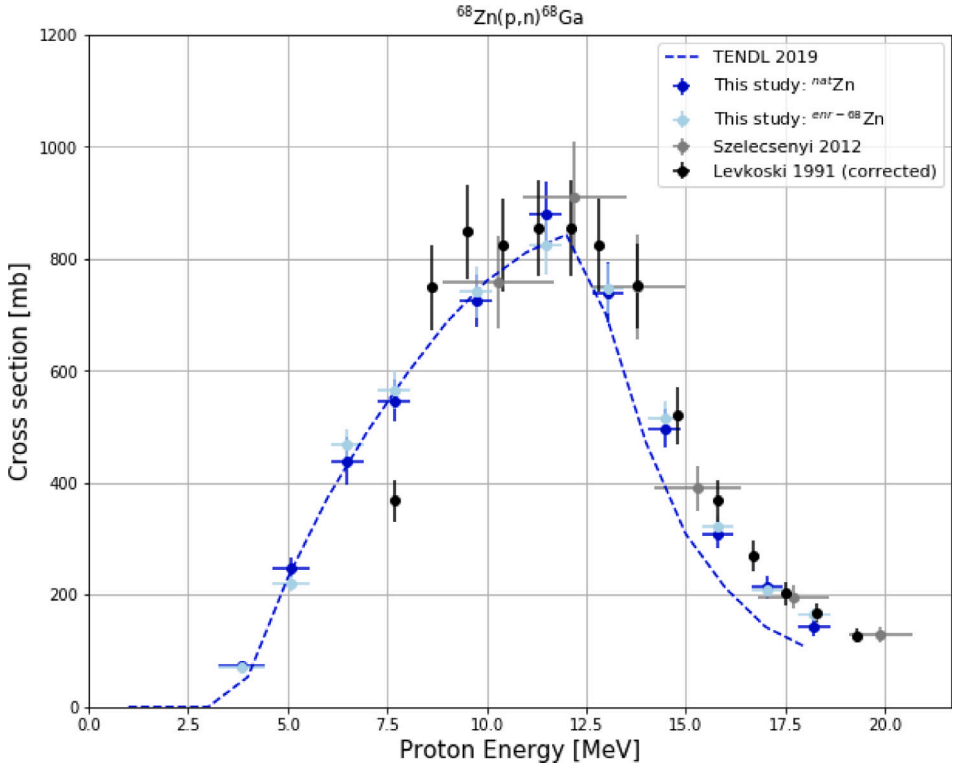


**Fig. 4.** $^{68}$Zn(p,n)$^{68}$Ga cross section measured from natural and enriched $^{68}$Zn targets with the isotopic composition marked as (A) in Table 1.

molten material or of any gas produced during the irradiation. The protons completely stop in the cup and do not activate the water of the cooling system.

For the production tests, a 99.26% enriched $^{68}$Zn metallic powder (marked as (B) in Table 1) and a 98.70% enriched $^{68}$Zn metallic foil (marked as (C) in Table 1) were used. In the former case, about 100 mg of material were pressed with a mass of 2.0 tons, resulting in a 0.5-mm thick 6-mm diameter pellet. In the latter case, discs with a diameter of 6 mm and a thickness of 0.2 mm were cut from the zinc foil and placed inside the coin pocket.

As the beam extracted from the cyclotron is ~12 mm FWHM at the position of the solid target station in standard irradiation conditions, only about 25% of the extracted protons are effectively used to produce the desired radionuclide if a 6 mm diameter pellet is used (Braccini et al., 2019). This produces an unwanted residual activity in the coin, giving rise to specific radiation protection measures and transport limitation. It also leads to the impossibility of precisely centering the beam, increasing the uncertainty on the integrated current and making the prediction of the produced activity difficult.

Therefore, to experimentally assess the activity produced at the End of Bombardment (EoB) before shipping the bulk material for further chemical processing, a system (Dellepiane et al., 2021) based on a 1 cm$^3$ CdZnTe (CZT) crystal was installed in the reception station. This detector allows the recording of energy spectra from the $\gamma$-rays emitted by the target. To optimize the response of the detector according to the activity, the position of the detector with respect to the source can be adjusted by means of an automatic motor, up to a maximum of about 50 cm. The low detection efficiency due to the distance and the small volume of the crystal makes this detector well suited for the measurement of high activities. This instrument has been experimentally calibrated by means of the previously-mentioned HPGe detector and allows the measurement of the activity with an accuracy of a few percent.

### 2.3. Study of $^{68}$Ga production yield and purity

Aiming at an optimized production of $^{68}$Ga, a study of the Thick Target Yield (TTY) and of the purity was performed. From the cross section measurements, the TTY for a given impinging proton energy $E$ can be calculated using the following formula:

$$TTY(E) = \frac{A(t_i)}{I \cdot t_i} = \frac{(1 - e^{-\lambda \cdot t_i})}{t_i} \cdot \frac{N_A \cdot \eta}{m_{mol} \cdot q} \int_{E_{th}}^{E} \frac{\sigma(E')}{S_p(E')} dE' \quad (2)$$

where $t_i$ is the irradiation time, $I$ the current on target, $A(t_i)$ the activity produced at EoB, $\lambda$ the decay constant, $\sigma(E')$ the cross-section as a function of the proton kinetic energy $E'$, $S_p(E')$ is the mass stopping power for the target material, $E_{th}$ is the threshold energy of the considered reaction, $N_A$ the Avogadro constant, $m_{mol}$ the average molar mass of the target material, $\eta$ the number of target atoms of the desired species per molecule and $q$ the charge of the projectile. The mass stopping power was calculated using SRIM.

For irradiation times $t_i$ much shorter with respect to the half-life, Eq. (2) can be approximated as:

$$TTY(E) \simeq \lambda \cdot \frac{N_A \cdot \eta}{m_{mol} \cdot q} \int_{E_{th}}^{E} \frac{\sigma(E')}{S_p(E')} dE' \quad (3)$$

If a thin target is used, so that the protons are not stopped therein, the production yield Y(E) can be defined as

$$Y(E) = TTY(E) - TTY(E_{out}) \quad (4)$$

where $E_{out}$ is the proton energy after the target, determined by using SRIM.

Given a sample containing a mixture of $N$ radioisotopes, the purity of the radionuclide of interest X is given by

$$P_X = \frac{A_X}{\sum_i^N A_i} \quad (5)$$

where $A_i$ is the activity of the $i$th radionuclide.

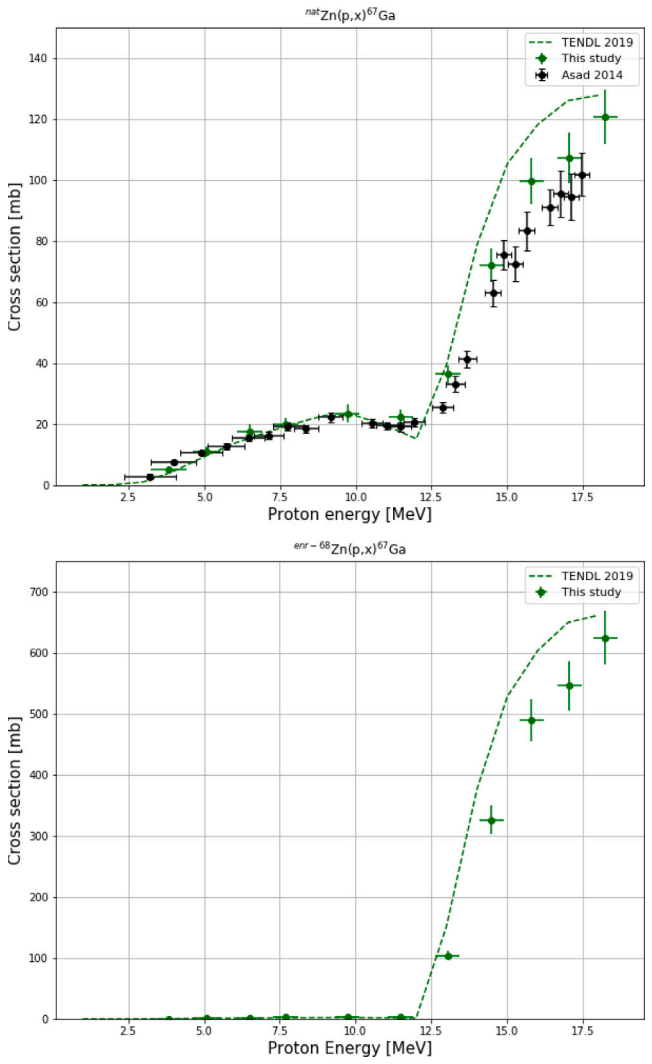


**Fig. 5.** Production cross section of $^{67}$Ga from $^{nat}$Zn (a) and $^{enr-68}$Zn (b) targets with the isotopic composition marked as (A) in Table 1.

## 3. Results

### 3.1. Cross-section measurements

The results of the $^{68}$Zn(p,n)$^{68}$Ga cross-section measurements, obtained from natural and enriched $^{68}$Zn (isotopic composition marked as (A) in Table 1) targets, are presented in Fig. 4; for completeness, the numerical values are reported in the Appendix ( Tables 5 and 6). Our measurements are in agreement with the experimental data available in the literature (Szelecsényi et al., 2012; Levkowskij, 1991) and are well reproduced by TENDL (Koning and Rochman, 2012). In accordance with the findings of Takács et Al. (Takacs et al., 2002), the values presented in (Levkowskij, 1991) were scaled by a factor of 0.8.

$^{67}$Ga is the main impurity that would be produced by irradiating an enriched $^{68}$Zn target. It is obtained from $^{68}$Zn and $^{67}$Zn via the reactions $^{68}$Zn(p,2n)$^{67}$Ga and $^{67}$Zn(p,n)$^{67}$Ga, respectively. The production cross sections measured from natural and enriched $^{68}$Zn zinc targets are reported in Fig. 5-a and Fig. 5-b, respectively. Our measurements are in agreement with the experimental data available in the literature (Asad et al., 2014) and are reasonably well reproduced by TENDL (Koning and Rochman, 2012). The nuclear reaction cross sections were calculated using the method described in Section 2.1 and are shown in Fig. 6. For completeness, the numerical values are reported in the Appendix (Tables 7 and 8). TENDL predictions are in reasonable agreement with our

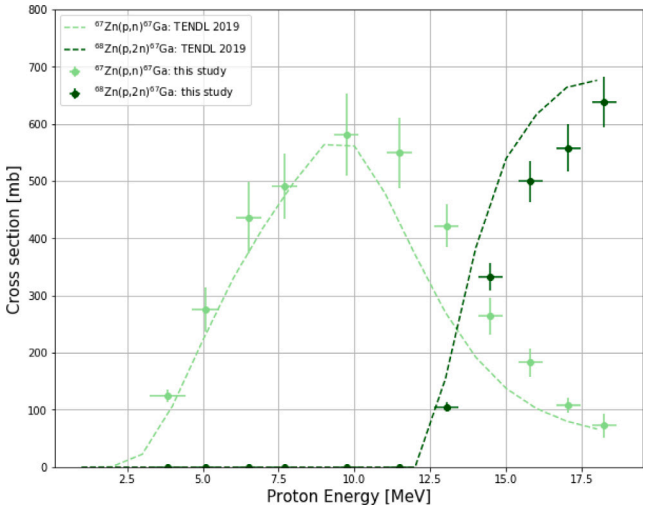


**Fig. 6.** $^{67}$Zn(p,n)$^{67}$Ga and $^{68}$Zn(p,2n)$^{67}$Ga reaction cross sections.

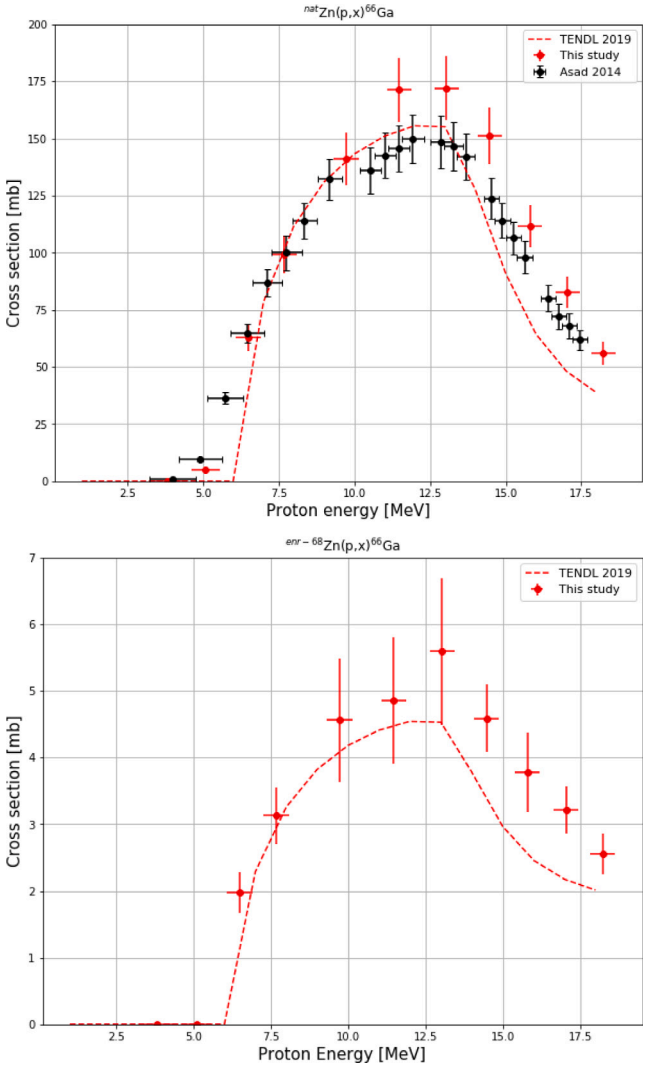


**Fig. 7.** Production cross section of $^{66}$Ga from $^{nat}$Zn (a) and $^{enr-68}$Zn (b) targets with the isotopic composition marked as (A) in Table 1.

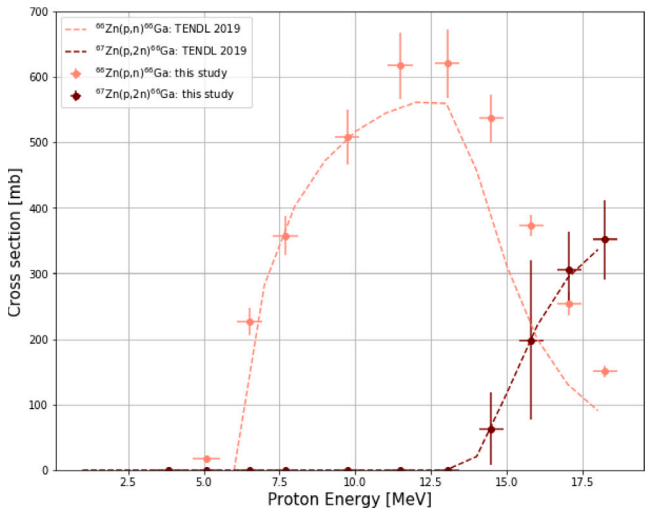


**Fig. 8.** $^{66}$Zn(p,n)$^{66}$Ga and $^{67}$Zn(p,2n)$^{66}$Ga reaction cross sections.

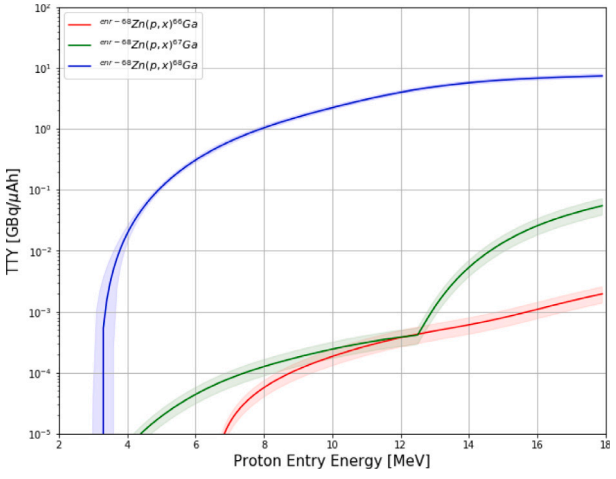


**Fig. 9.** $^{68}$Ga, $^{67}$Ga and $^{66}$Ga thick target yields for a 99.26% enriched $^{68}$Zn target for an irradiation time $t_i$ of one hour. The bands correspond to the maximum and minimum yield calculated on the basis of the measured cross-sections.

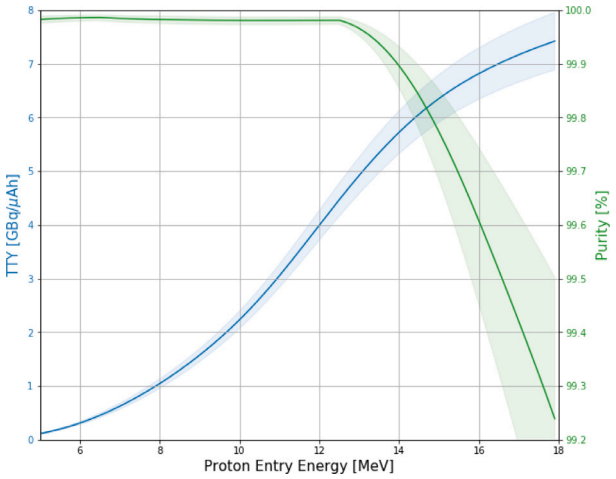


**Fig. 10.** $^{68}$Ga thick target yield and purity for a 99.26% enriched $^{68}$Zn target for an irradiation time $t_i$ of one hour. The bands correspond to the maximum and minimum yield calculated on the basis of the measured cross-sections.

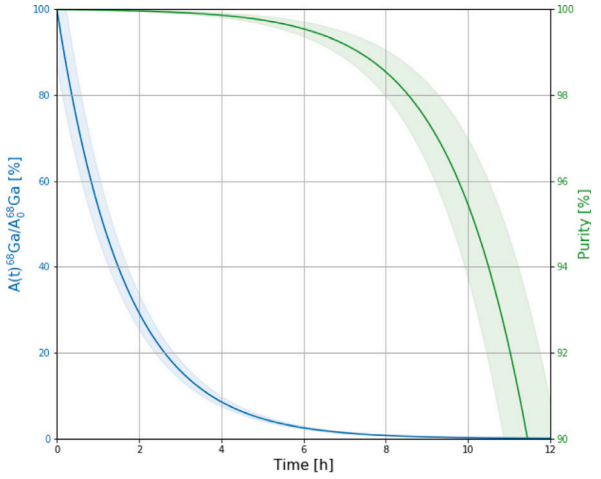


**Fig. 11.** $^{68}$Ga activity fraction and purity as a function of time after EoB for a 99.26% enriched $^{68}$Zn target. The bands correspond to the maximum and minimum activity calculated on the basis of the measured cross-sections.

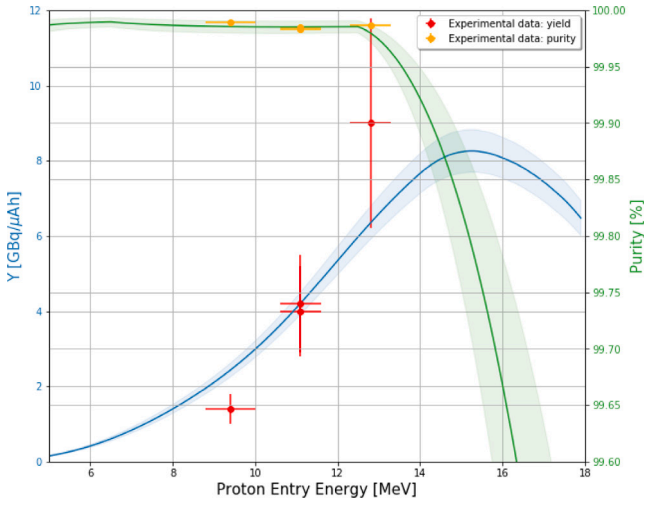


(a)

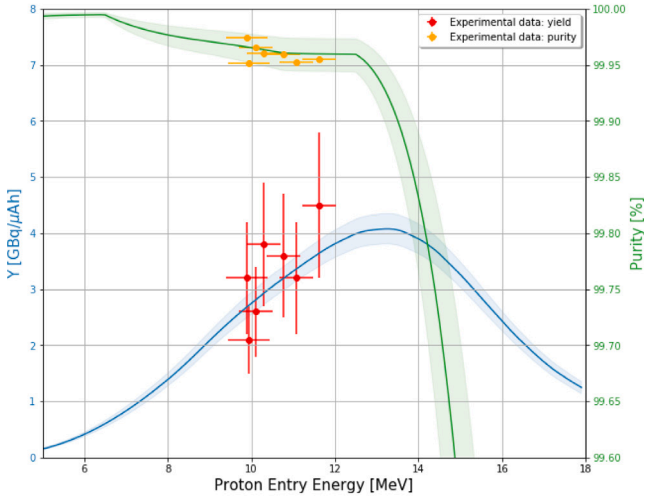


(b)

**Fig. 12.** $^{68}$Ga production yield and purity calculated from the measured cross-sections in our irradiation conditions compared to the experimental results for the 0.5-mm-thick 99.26% enriched $^{68}$Zn pellet (a) and the 0.2-mm-thick 98.70% enriched $^{68}$Zn discs (b). The bands correspond to the maximum and minimum yield calculated on the basis of the measured cross-sections.

**Table 3**
Irradiation parameters, $^{68}$Ga activity, yield, purity and radioisotopic impurities at EoB obtained irradiating the 0.5-mm-thick pellet (isotopic composition marked as (B) in Table 1). The values in parentheses are the yield calculations based on the cross section measurements.

| | $E_{in}$ [MeV] | Charge [μAh] | Y($^{68}$Ga) [GBq/μAh] | Y($^{67}$Ga) [MBq/μAh] | Y($^{66}$Ga) [MBq/μAh] | P($^{68}$Ga) [%] |
|---|---|---|---|---|---|---|
| Irradiation 1 | 9.4 ± 0.6 | (0.87 ± 0.26)·10$^{-3}$ | 1.4 ± 0.4 *(2.4)* | 0.11 ± 0.03 *(0.20)* | 0.04 ± 0.01 *(0.14)* | 99.9891 ± 0.0004 *(99.9856)* |
| Irradiation 2 | 11.1 ± 0.5 | 0.56 ± 0.17 | 4.0 ± 1.2 *(4.7)* | 0.34 ± 0.10 *(0.35)* | 0.27 ± 0.08 *(0.34)* | 99.9848 ± 0.0010 *(99.9854)* |
| Irradiation 3 | 11.1 ± 0.5 | 3.07 ± 0.92 | 4.2 ± 1.3 *(4.7)* | 0.40 ± 0.12 *(0.35)* | 0.30 ± 0.09 *(0.34)* | 99.9834 ± 0.0014 *(99.9854)* |
| Irradiation 4 | 12.8 ± 0.5 | 0.12 ± 0.03 | 9.0 ± 2.7 *(6.3)* | 0.63 ± 0.19 *(0.80)* | 0.58 ± 0.18 *(0.48)* | 99.9864 ± 0.0010 *(99.9798)* |

**Table 4**
Irradiation parameters, $^{68}$Ga activity, yield, purity and radioisotopic impurities at EoB obtained irradiating the 0.2 mm thick discs (isotopic composition listed as (C) in Table 1). The values in parentheses are the yield calculations based on the cross section measurements.

| | $E_{in}$ [MeV] | Charge [μAh] | Y($^{68}$Ga) [GBq/μAh] | Y($^{67}$Ga) [MBq/μAh] | Y($^{66}$Ga) [MBq/μAh] | P($^{68}$Ga) [%] |
|---|---|---|---|---|---|---|
| Irradiation 1 | 9.9 ± 0.6 | 1.90 ± 0.57 | 3.2 ± 1.0 *(2.7)* | 0.12 ± 0.04 *(0.11)* | 0.7 ± 0.2 *(0.8)* | 99.9743 ± 0.0003 *(99.9663)* |
| Irradiation 2 | 9.9 ± 0.6 | 1.87 ± 0.56 | 2.1 ± 0.6 *(2.7)* | 0.10 ± 0.03 *(0.10)* | 0.9 ± 0.3 *(0.8)* | 99.9508 ± 0.0011 *(99.9660)* |
| Irradiation 3 | 10.1 ± 0.5 | 0.54 ± 0.16 | 2.6 ± 0.8 *(2.8)* | 0.11 ± 0.03 *(0.11)* | 0.8 ± 0.2 *(0.9)* | 99.9657 ± 0.0009 *(99.9657)* |
| Irradiation 4 | 10.3 ± 0.5 | 0.28 ± 0.08 | 3.8 ± 1.1 *(2.9)* | 0.14 ± 0.04 *(0.11)* | 1.4 ± 0.4 *(1.0)* | 99.9603 ± 0.0005 *(99.9603)* |
| Irradiation 5 | 10.8 ± 0.5 | 0.16 ± 0.05 | 3.6 ± 1.1 *(3.2)* | 0.14 ± 0.04 *(0.12)* | 1.3 ± 0.4 *(1.1)* | 99.9593 ± 0.0008 *(99.9593)* |
| Irradiation 6 | 11.1 ± 0.5 | 1.16 ± 0.35 | 3.1 ± 0.9 *(3.4)* | 0.13 ± 0.04 *(0.12)* | 1.4 ± 0.4 *(1.2)* | 99.9520 ± 0.0007 *(99.9520)* |
| Irradiation 7 | 11.6 ± 0.5 | 0.24 ± 0.07 | 4.5 ± 1.4 *(3.7)* | 0.16 ± 0.05 *(0.12)* | 1.9 ± 0.6 *(1.3)* | 99.9549 ± 0.0007 *(99.9549)* |

data. As concerns $^{66}$Ga, it is obtained from $^{67}$Zn and $^{66}$Zn via the $^{67}$Zn(p,2n)$^{66}$Ga and $^{66}$Zn(p,n)$^{66}$Ga reactions, respectively. The production cross sections measured from natural and enriched $^{68}$Zn targets are reported in Fig. 7-a and Fig. 7-b, respectively. Our measurements are in agreement with the experimental data available in the literature (Asad et al., 2014) and are well reproduced by TENDL (Koning and Rochman, 2012). The nuclear reaction cross sections are shown in Fig. 8, and for completeness, the numerical values are reported in the Appendix (Tables 9 and 10). TENDL predictions are in reasonable agreement with our data.

For the $^{68}$Zn(p,n)$^{68}$Ga, $^{nat}$Zn(p,X)$^{67}$Ga and $^{enr\text{-}68}$Zn(p,X)$^{67}$Ga reactions, the main experimental uncertainty was due to the flatness of the beam (about 5%). Other sources of uncertainty include the integrated beam current (~1%), the HPGe detector efficiency (3%) and the target mass measurements (up to 3%). For the reactions $^{nat}$Zn(p,X)$^{66}$Ga and $^{enr\text{-}68}$Zn(p,X)$^{66}$Ga the main experimental uncertainty was due to the branching ratio (5.4%) of the 1039 keV $\gamma$-ray. The $\gamma$-branching ratio was a negligible source of uncertainty for the other reactions. The total uncertainty is obtained by summing all the contributions in quadrature. The energy spread was simulated using SRIM and was taken into account to calculate the uncertainty on the beam energy. The contribution due to the aluminum absorber was summed in quadrature with the energy spread of the pristine beam. The overall energy spread ranges from 0.4 MeV (no absorbers) to 0.6 MeV (with a 1675 μm absorber and the 13 μm Al cover foil, bringing the energy on target down to 3.8 MeV).

### 3.2. Production with solid targets

A study of the production yield (Y) and the purity was performed in order to optimize the $^{68}$Ga production. Given the results obtained for nuclear cross sections, it is possible to calculate the production yield for any enriched material. As an example, the thick-target production yields (Eq. (2)) of $^{68}$Ga, $^{67}$Ga and $^{66}$Ga using the 99.26% enriched $^{68}$Zn target material (marked as (B) in Table 1) are shown in Fig. 9 as a function of the impinging proton energy. The irradiation time $t_i$ is set to one hour. The fraction of $^{68}$Ga produced and the presence of the main impurity $^{67}$Ga strongly depend on the energy of the proton beam entering the target, as reported in Fig. 10, where the purity is calculated according to Eq. (5). In particular, the threshold for the nuclear reaction $^{68}$Zn(p,2n)$^{67}$Ga lies at around 12 MeV (Fig. 6); high-purity $^{68}$Ga can therefore be obtained only at energies below this value at the expense of the yield.

Considering an optimal impinging energy of 11.5 MeV, the radionuclidic purity as a function of time can be calculated, as shown in Fig. 11, where the fraction of the remaining $^{68}$Ga activity is reported. From the plot, it results that the purity remains above 98% up to more than eight hours after EoB. Within this time, the synthesis of the radiopharmaceutical and its subsequent injection into the patient have to take place to fulfill the requirements of the European Pharmacopoeia.

The degradation of the proton beam to the desired energy can be obtained by choosing the material and thickness of the window foil in the STS, which separates the cyclotron vacuum from the helium cooling chambers. Furthermore, the thickness of the front part of the coin lid can also be adjusted.

Two series of $^{68}$Ga production tests were performed at different proton energies in the range (9–13) MeV, irradiating the 0.5-mm-thick enriched $^{68}$Zn pellet (isotopic composition marked as (B) in Table 1) and the 0.2-mm-thick enriched $^{68}$Zn discs (isotopic composition marked as (C) in Table 1). The irradiation time $t_i$ was kept below 30 min so that Eq. (3) can be used to calculate the TTY. After each irradiation

**Table 5**
$^{68}$Ga production cross sections measured from natural and enriched $^{68}$Zn (marked as (A) in Table 1) targets.

| E [MeV] | $^{nat}$Zn(p,x)$^{68}$Ga [mbarn] | $^{enr-68}$Zn(p,x)$^{68}$Ga [mbarn] |
|---|---|---|
| 3.8 ± 0.6 | 14 ± 1 | 69 ± 4 |
| 5.1 ± 0.5 | 46 ± 3 | 215 ± 13 |
| 6.5 ± 0.4 | 81 ± 8 | 457 ± 28 |
| 7.7 ± 0.4 | 101 ± 7 | 554 ± 33 |
| 9.7 ± 0.4 | 134 ± 9 | 724 ± 45 |
| 11.5 ± 0.4 | 163 ± 10 | 807 ± 52 |
| 13.0 ± 0.4 | 136 ± 10 | 731 ± 44 |
| 14.5 ± 0.4 | 92 ± 6 | 505 ± 30 |
| 15.8 ± 0.4 | 57 ± 5 | 314 ± 19 |
| 17.1 ± 0.4 | 39 ± 4 | 205 ± 14 |
| 18.2 ± 0.4 | 26 ± 3 | 163 ± 10 |

**Table 6**
$^{68}$Zn(p,n)$^{68}$Ga reaction cross sections measured from natural and enriched $^{68}$Zn (marked as (A) in Table 1) targets.

| E [MeV] | $^{68}$Zn(p,n)$^{68}$Ga (nat) [mbarn] | $^{68}$Zn(p,n)$^{68}$Ga (enr) [mbarn] |
|---|---|---|
| 3.8 ± 0.6 | 74 ± 6 | 71 ± 4 |
| 5.1 ± 0.5 | 249 ± 18 | 220 ± 13 |
| 6.5 ± 0.4 | 439 ± 43 | 467 ± 29 |
| 7.7 ± 0.4 | 547 ± 37 | 566 ± 34 |
| 9.7 ± 0.4 | 725 ± 48 | 741 ± 46 |
| 11.5 ± 0.4 | 881 ± 56 | 825 ± 53 |
| 13.0 ± 0.4 | 739 ± 54 | 748 ± 45 |
| 14.5 ± 0.4 | 497 ± 34 | 516 ± 30 |
| 15.8 ± 0.4 | 309 ± 25 | 322 ± 20 |
| 17.1 ± 0.4 | 214 ± 20 | 209 ± 14 |
| 18.2 ± 0.4 | 142 ± 16 | 166 ± 10 |

**Table 7**
$^{67}$Ga production cross sections measured from natural and enriched $^{68}$Zn (marked as (A) in Table 1) targets.

| E [MeV] | $^{nat}$Zn(p,x)$^{67}$Ga [mbarn] | $^{enr-68}$Zn(p,x)$^{67}$Ga [mbarn] |
|---|---|---|
| 3.8 ± 0.6 | 5.0 ± 0.5 | 0.4 ± 0.1 |
| 5.1 ± 0.5 | 11 ± 2 | 0.8 ± 0.3 |
| 6.5 ± 0.4 | 18 ± 3 | 1.9 ± 0.6 |
| 7.7 ± 0.4 | 20 ± 2 | 2.4 ± 0.8 |
| 9.7 ± 0.4 | 23 ± 3 | 2.8 ± 0.6 |
| 11.5 ± 0.4 | 22 ± 2 | 3.1 ± 0.8 |
| 13.0 ± 0.4 | 36 ± 3 | 104 ± 8 |
| 14.5 ± 0.4 | 72 ± 6 | 326 ± 23 |
| 15.8 ± 0.4 | 100 ± 8 | 489 ± 35 |
| 17.1 ± 0.4 | 107 ± 8 | 546 ± 41 |
| 18.2 ± 0.4 | 121 ± 9 | 625 ± 43 |

**Table 8**
$^{67}$Zn(p,n)$^{67}$Ga and $^{68}$Zn(p,2n)$^{67}$Ga reaction cross sections.

| E [MeV] | $^{67}$Zn(p,n)$^{67}$Ga [mbarn] | $^{68}$Zn(p,2n)$^{67}$Ga [mbarn] |
|---|---|---|
| 3.8 ± 0.6 | 125 ± 12 | No signal |
| 5.1 ± 0.5 | 276 ± 39 | No signal |
| 6.5 ± 0.4 | 435 ± 63 | No signal |
| 7.7 ± 0.4 | 490 ± 57 | No signal |
| 9.7 ± 0.4 | 580 ± 72 | No signal |
| 11.5 ± 0.4 | 549 ± 62 | No signal |
| 13.0 ± 0.4 | 422 ± 38 | 105 ± 8 |
| 14.5 ± 0.4 | 264 ± 32 | 333 ± 23 |
| 15.8 ± 0.4 | 183 ± 25 | 499 ± 35 |
| 17.1 ± 0.4 | 107 ± 13 | 558 ± 42 |
| 18.2 ± 0.4 | 72 ± 22 | 638 ± 44 |

**Table 9**
$^{66}$Ga production cross sections measured from natural and enriched $^{68}$Zn (marked as (A) in Table 1) targets.

| E [MeV] | $^{nat}$Zn(p,x)$^{66}$Ga [mbarn] | $^{enr-68}$Zn(p,x)$^{66}$Ga [mbarn] |
|---|---|---|
| 3.8 ± 0.6 | No signal | No signal |
| 5.1 ± 0.5 | 5 ± 1 | No signal |
| 6.5 ± 0.4 | 63 ± 6 | 2.0 ± 0.3 |
| 7.7 ± 0.4 | 99 ± 8 | 3.1 ± 0.4 |
| 9.7 ± 0.4 | 141 ± 12 | 4.6 ± 0.9 |
| 11.5 ± 0.4 | 171 ± 14 | 4.9 ± 0.9 |
| 13.0 ± 0.4 | 172 ± 15 | 6 ± 1 |
| 14.5 ± 0.4 | 151 ± 12 | 4.6 ± 0.5 |
| 15.8 ± 0.4 | 112 ± 9 | 3.8 ± 0.6 |
| 17.1 ± 0.4 | 83 ± 7 | 3.2 ± 0.4 |
| 18.2 ± 0.4 | 56 ± 5 | 2.6 ± 0.3 |

the pellet was let to decay completely. The entry energies, the irradiation parameters and the activities obtained from the two series of measurements are reported in Tables 3 and 4.

The production yield of $^{68}$Ga calculated in our irradiation conditions from Eq. (4) and the experimental results are shown in Fig. 12 as a function of the proton energy. A good agreement was found between the experimental data and the predictions based on our cross-sections. The main contribution to the experimental uncertainty is given by the uncertainty on the integrated current, which is about 30%.

## 4. Conclusions and outlook

The interest for the use of $^{68}$Ga for PET diagnostics in nuclear medicine is increasing. In particular, this radionuclide can be exploited for theranostics because it can be used to label relevant biomolecules such as proteins and peptides, making it a good diagnostic partner for the therapeutic radiolanthanide $^{177}$Lu.

To enhance the availability of $^{68}$Ga, cyclotron production with solid targets represents a very promising option. To select the optimal irradiation conditions, the cross section of the $^{68}$Zn(p,n)$^{68}$Ga nuclear reaction was measured at the Bern University Hospital cyclotron laboratory, irradiating both natural and enriched $^{68}$Zn zinc targets. Despite the use of a highly enriched target material, $^{67}$Ga and $^{66}$Ga impurities are also produced and, having longer half-lives with respect to $^{68}$Ga, cannot be removed from the sample by decay time. For this reason, the accurate knowledge of all cross sections is of paramount importance to determine the beam energy leading to the optimal $^{68}$Ga production yield and radionuclidic purity. Along this line, the production of $^{67}$Ga and $^{66}$Ga was studied and the corresponding nuclear reaction cross sections measured.

Several production tests were successfully performed irradiating 99.26% and 98.70% enriched $^{68}$Zn targets with a solid target station. Using the optimal impinging energy of 11.5 MeV, a $^{68}$Ga yield of 4.2 GBq/μAh with a radioisotopic purity of 99.98% was achieved at EoB. We proved that in this case the purity remains above 98% until about 8 h after EoB. Within this period, the synthesis of the radiopharmaceutical and its subsequent injection into the patient have to take place to fulfill the requirements of the European Pharmacopoeia.

These results are in line with previous findings (IAEA, 2019) and confirm the excellent prospects for the production of $^{68}$Ga with medical cyclotrons, paving the way towards its widespread use for PET diagnostics and theranostic in nuclear medicine.

**Table 10**
$^{66}$Zn(p,n)$^{66}$Ga and $^{67}$Zn(p,2n)$^{66}$Ga reaction cross sections.

| E [MeV] | $^{66}$Zn(p,n)$^{66}$Ga [mbarn] | $^{67}$Zn(p,2n)$^{66}$Ga [mbarn] |
|---|---|---|
| 3.8 ± 0.6 | No signal | No signal |
| 5.1 ± 0.5 | 18 ± 3 | No signal |
| 6.5 ± 0.4 | 226 ± 21 | No signal |
| 7.7 ± 0.4 | 358 ± 30 | No signal |
| 9.7 ± 0.4 | 509 ± 42 | No signal |
| 11.5 ± 0.4 | 618 ± 51 | No signal |
| 13.0 ± 0.4 | 620 ± 53 | No signal |
| 14.5 ± 0.4 | 537 ± 36 | 63 ± 56 |
| 15.8 ± 0.4 | 373 ± 16 | 198 ± 122 |
| 17.1 ± 0.4 | 254 ± 17 | 306 ± 57 |
| 18.2 ± 0.4 | 150 ± 9 | 352 ± 60 |

## CRediT authorship contribution statement

**S. Braccini:** Writing – review & editing, Writing – original draft, Visualization, Validation, Supervision, Resources, Project administration, Methodology, Investigation, Funding acquisition, Conceptualization. **T.S. Carzaniga:** Writing – review & editing, Investigation, Formal analysis, Data curation. **G. Dellepiane:** Writing – review & editing, Writing – original draft, Software, Methodology, Investigation, Formal analysis, Data curation, Conceptualization. **P.V. Grundler:** Writing – review & editing, Investigation. **P. Scampoli:** Writing – review & editing, Writing – original draft, Visualization, Validation, Investigation. **N.P. van der Meulen:** Writing – review & editing, Validation, Methodology, Investigation. **D. Wüthrich:** Writing – review & editing, Investigation, Formal analysis, Data curation.

## Declaration of competing interest

The authors declare that they have no known competing financial interests or personal relationships that could have appeared to influence the work reported in this paper.

## Acknowledgments

We acknowledge contributions from LHEP engineering and technical staff (Roger Hänni and Jan Christen, in particular). We are thankful to the SWAN Isotopen AG maintenance team (Riccardo Bosi and Michel Eggemann, in particular) for the collaboration in the set-up and operation of the solid target system. This research project was partially funded by the Swiss National Science Foundation (SNSF) (grants: CR23I2_156852, 200021_175749 and CRSII5_180352).

## Appendix

See Tables 5–10.

## References

Alnahwi, A.H., Tremblay, S., Ait-Mohand, S., Beaudoin, J.F., Guérin, B., 2020. Automated radiosynthesis of $^{68}$Ga for large-scale routine production using $^{68}$Zn pressed target. Appl. Radiat. Isot. 156, 109014. http://dx.doi.org/10.1016/j.apradiso.2019.109014.

Alves, F., Alves, V.H., Neves, A.C.B., 2017. Cyclotron production of $^{68}$Ga for human use from liquid targets: From theory to practice. AIP Conf. Proc. 1845 1, 020001. http://dx.doi.org/10.1063/1.4983532.

Anon, 2021. Gallium ($^{68}$Ga) chloride (accelerator-produced) solution for radiolabelling. Eur. Pharm. 10.3, 4864–4865.

Asad, A.H., Chan, S., Morandeau, L., Cryer, D., Smith, S.V., Price, R.I., 2014. Excitation functions of natZn(p,x) nuclear reactions with proton beam energy below 18 MeV. Appl. Radiat. Isot. 94, 67–71. http://dx.doi.org/10.1016/j.apradiso.2014.07.008.

Auger, M., Braccini, S., Carzaniga, T.S., Ereditato, A., Nesteruk, K.P., Scampoli, P., 2016. A detector based on silica fibers for ion beam monitoring in a wide current range. J. Instrum. 11 (03), P03027. http://dx.doi.org/10.1088/1748-0221/11/03/p03027.

Braccini, S., 2013. The new bern PET cyclotron, its research beam line, and the development of an innovative beam monitor detector. AIP Conf. Proc. 1525, 144–150. http://dx.doi.org/10.1063/1.4802308.

Braccini, S., Aguilar, C.B., Carzaniga, T.S., Dellepiane, G., Häffner, P.D., Scampoli, P., 2019. Novel irradiation methods for theranostic radioisotope production with solid targets at the bern medical cyclotron. In: Proceedings of Cyclotrons2019. http://dx.doi.org/10.18429/JACoW-Cyclotrons2019-TUA02.

Braccini, S., Scampoli, P., 2016. Science with a medical cyclotron. CERN Courier April 2016, 21–22.

Carzaniga, T.S., Auger, M., Braccini, S., Bunka, M., Ereditato, A., Nesteruk, K.P., Scampoli, P., Türler, A., van der Meulen, N.P., 2017. Measurement of $^{43}$Sc and $^{44}$Sc production cross-section with an 18 MeV medical PET cyclotron. Appl. Radiat. Isot. 129, 96–102. http://dx.doi.org/10.1016/j.apradiso.2017.08.013.

Carzaniga, T.S., Braccini, S., 2019. Cross-section measurement of $^{44m}$Sc, $^{47}$Sc, $^{48}$Sc and $^{47}$Ca for an optimized$^{47}$Sc production with an 18 MeV medical PET cyclotron. Appl. Radiat. Isot. 143, 18–23. http://dx.doi.org/10.1016/j.apradiso.2018.10.015.

Dellepiane, G., Aguilar, C.B., Carzaniga, T.S., Casolaro, P., Häffner, P., Scampoli, P., Schmid, M., Braccini, S., 2021. Research on theranostic radioisotope production at the bern medical cyclotron. IL Nuovo Cimento C 44, http://dx.doi.org/10.1393/ncc/i2021-21130-6.

Dellepiane, G., Casolaro, P., Favaretto, C., Grundler, P.V., Mateu, I., Scampoli, P., Talip, Z., van der Meulen, N.P., Braccini, S., 2022. Cross section measurement of terbium radioisotopes for an optimized $^{155}$tb production with an 18 mev medical pet cyclotron. Applied Radiation and Isotopes (ISSN: 0969-8043) 184, 110175. http://dx.doi.org/10.1016/j.apradiso.2022.110175.

Favaretto, C., Talip, Z., Borgna, F., Grundler, P.V., Dellepiane, G., Sommerhalder, A., Zhang, H., Schibli, R., Braccini, S., Müller, C., van der Meulen, N.P., 2021. Cyclotron production and radiochemical purification of terbium-155 for SPECT imaging. EJNMMI Radiopharm. Chem. 6, 37. http://dx.doi.org/10.1186/s41181-021-00153-w.

Häffner, P.D., Aguilar, C.B., Braccini, S., Scampoli, P., Thonet, P.A., 2019. Study of the extracted beam energy as a function of operational parameters of a medical cyclotron. Instruments 3 (4), 63. http://dx.doi.org/10.3390/instruments3040063.

IAEA, 2019. Gallium-68 Cyclotron Production. In: TECDOC Series, (1863), Vienna.

IAEA, 2021. Live chart of nuclides, available online. URL https://nds.iaea.org/relnsd/vcharthtml/vcharthtml.html. Last Access 27 December 2021.

Koning, A., Rochman, D., 2012. Modern nuclear data evaluation with the TALYS code system. Nucl. Data Sheets 113, 2841–2934. http://dx.doi.org/10.1016/j.nds.2012.11.002.

Levkowskij, V., 1991. Activation cross sections for the nuclides of Medium Mass Region (A=40-100) with Protons and $\alpha$-particles at Medium (E=10-50 MeV) energies. Inter-Vesti, Moscow.

Nelson, B.J.B., Wilson, J., Richter, S., Duke, M.J.M., Wuest, M., Wuest, F., 2020. Taking cyclotron $^{68}$Ga production to the next level: Expeditious solid target production of $^{68}$Ga for preparation of radiotracers. Nucl. Med. Biol. 80–81, 24–31. http://dx.doi.org/10.1016/j.nucmedbio.2020.01.005.

Nesteruk, K., Auger, M., Braccini, S., Carzaniga, T., Ereditato, A., Scampoli, P., 2018. A system for online beam emittance measurements and proton beam characterization. J. Instrum. 13 (01), P01011. http://dx.doi.org/10.1088/1748-0221/13/01/P01011.

Potkins, D.E., Braccini, S., Nesteruk, K.P., Carzaniga, T.S., Vedda, A., Chiodini, N., Timmermans, J., Melanson, S., Dehnel, M.P., 2017. A low-cost beam profiler based on cerium-doped silica fibers. In: Proceedings of CAARI-16, Physics Procedia. http://dx.doi.org/10.1016/j.phpro.2017.09.061.

Riga, S., Cicoria, G., Pancaldi, D., 2018. Production of $^{68}$Ga with a general electric PETtrace cyclotron by liquid target. Phys. Medica 55, 116–126. http://dx.doi.org/10.1016/j.ejmp.2018.10.018.

Sadeghi, M., Kakavand, T., Rajabifar, S., Mokhtari, L., Rahimi-Nezhad, A., 2009. Cyclotron production of $^{68}$Ga via proton-induced reaction on $^{68}$Zn target. Nucleonika 54 (1), 25–28.

Szelecsényi, F., Kovács, Z., Nagatsu, K., Fukumura, K., Suzuki, K., Mukai, K., 2012. Investigation of direct production of $^{68}$Ga with low energy multiparticle accelerator. Radiochim. Acta 100, 5–11. http://dx.doi.org/10.1524/ract.2011.1896.

Takacs, S., Tarkanyi, F., Sonck, M., Hermanne, A., 2002. Investigation of the $^{nat}$Mo(p,x)$^{96mg}$Tc nuclear reaction to monitor proton beams: New measurements and consequences on the earlier reported data. Nucl. Instrum. Methods Phys. Res. B 198, 183–196.

van der Meulen, N.P., Hasler, R., Talip, Z., Grundler, P.V., Favaretto, C., Umbricht, C.A., Müller, C., Dellepiane, G., Carzaniga, T.S., Braccini, S., 2020. Developments toward the implementation of $^{44}$Sc production at a medical cyclotron. Molecules 25, 1–16. http://dx.doi.org/10.3390/molecules25204706.

Ziegler, J.F., Manoyan, J.M., 2013. The stopping of ions in compounds. Nucl. Instrum. Methods B 35, 215, URL http://www.srim.org.